JACS
JOURNAL OF THE AMERICAN CHEMICAL SOCIETY
pubs.acs.org/JACS
Article

Orientational Geometry, Surface Density, and Binding Free Energy of Intermediates as Full Descriptors for Electrochemical CO_2 Reduction at Metal Surfaces

Hui Wang, Haley Fisher, Zhi-Chao Huang-Fu,* Jesse B. Brown, Tong Zhang, Fuzhan Song, Yuqin Qian, and Yi Rao*

Cite This: J. Am. Chem. Soc. 2025, 147, 19101−19112

Read Online

ACCESS | Metrics & More | Article Recommendations | Supporting Information

ABSTRACT: Metal catalysts for the electrochemical CO_2 reduction reaction (CO_2RR) have attracted widespread attention due to their high catalytic efficiency, stability, broad product diversity, and ease of preparation. Studies show that the product distribution and yield of the electrochemical CO_2RR on metal surfaces result from the metal's binding energy of an intermediate adsorbed CO (*CO). However, reaction pathways could be manipulated by other thermodynamic parameters, such as orientation and surface density. In this work, the CO_2RR on Au electrode surfaces was comprehensively analyzed using high-performance *in situ* electrochemical sum-frequency generation (EC-SFG) spectroscopy. The improved signal intensities allowed the reaction to be monitored with a fast time resolution, extracting key thermodynamic and kinetic features from the experiments. Our EC-SFG spectrometer allowed the comprehensive analysis of the potential-dependent polarized SFG signal, allowing us to quantify *CO orientation at the Au electrode surface as a function of applied potential. These experimental results were then used to determine the maximum surface density and binding energies of the *CO intermediate in a self-contained analysis. These EC-SFG experiments enabled us to quantify the reaction rate constant for the system. We then discuss how the binding energy, orientation angle, and absolute surface density of an intermediate should be fully considered in understanding its thermodynamic behaviors in the CO_2RR. This work demonstrates the potential of high-efficiency EC-SFG spectroscopy to provide an all-inclusive analysis of the CO_2RR on metal surfaces and opens the door for other catalysts to be investigated using this technique to determine the best system for efficient electrocatalysis.

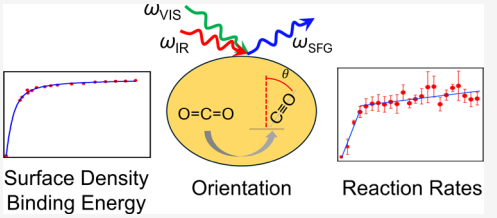

1. INTRODUCTION

The global energy and climate crises call for robust methods of clean energy production and greenhouse gas emission reduction/sequestration, resulting in a surge of research in the field.[1] A possible solution is the electrochemical CO_2 reduction reaction (CO_2RR) to convert CO_2 into clean and renewable energy sources and starting materials.[2] However, the stability of CO_2 results in a necessary high overpotential, which complicates its reduction process.[3] Catalytic solutions are often unstable, have low faradic efficiency (FE), and compete with the hydrogen evolution reaction (HER).[4,5] For these reasons, a better understanding of CO_2RR mechanisms for different electrodes is vital to overcome these obstacles and increase efficiency, and a good starting point may be with metal electrocatalysts.[2,6]

Previous studies have shown that the product distribution and yield of the CO_2RR on metal electrodes are mainly affected by the binding energy of the intermediate adsorbed CO (*CO).[7,8] Binding energy reflects the strength with which the electrodes hold the *CO to its surface and requires a careful balance for the reaction to proceed efficiently.[9−11] If the intermediate is bound too tightly, it can inhibit reaction progress; however, too weak binding can result in *CO easily being released before further reactions can occur. For example, Pt binds strongly to *CO, resulting in fewer CO_2RR products because the catalytic sites are occupied by *CO, resulting in hydrogen gas being the primary product. However, metals with intermediate binding energy, such as Cu, further reduce the *CO into alcohols and hydrocarbons, which creates a complex system with many possible pathways.[12−14] Continuing the pattern, Au binds *CO weakly and as a result produces mostly CO because it is released from the surface before it can be further reduced.[4,5,15−18] Even though investigations into CO_2RR on Au-based catalysts have been documented for years,[19−26] they are still the most active and selective materials for the generation of CO. As such, understanding the CO_2RR mechanism of Au-based catalysts can better inform research on new catalyst materials.

Received: March 11, 2025
Revised: May 14, 2025
Accepted: May 16, 2025
Published: May 27, 2025

Downloaded via TSINGHUA UNIV on June 16, 2025 at 13:10:59 (UTC).
See https://pubs.acs.org/sharingguidelines for options on how to legitimately share published articles.

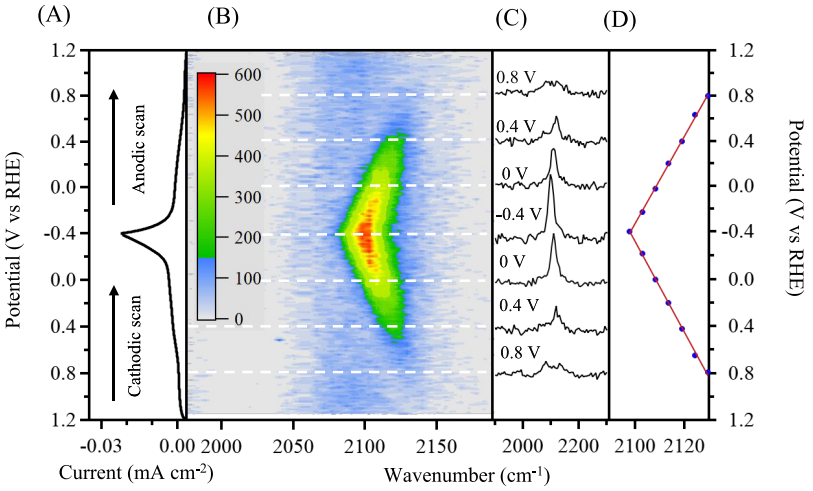

Figure 1. (A) Cyclic voltammogram of Au in 0.1 M $KHCO_3$ saturated with CO_2 at 5 mV s^{-1} from 1.2 to −0.4 to 1.2 V; (B) EC-SFG map at PPP polarization at Au surface as a function of applied potential using a collection time of 2 s; (C) representative SFG spectra at different applied potentials; (D) Stark effect of *CO vibration under PPP polarization from 1.2 to −0.4 to 1.2 V. Blue dots represent experimental data, and red solid lines are to guide the eye. Horizontal dashed lines correlate the data in (B) to its component parts in (A−D).

In addition to binding energy, intermediate orientation and surface density can affect the electrochemical reaction.[12−14,27,28] For instance, the presence of solvated cations at gold surfaces was shown to increase local CO_2 concentration, which in turn increased reaction efficiency due to increased CO_2 surface density.[29] The surface density can also affect reaction product yield, where different crystal structures of Cu electrodes resulted in increased *CO presence, promoting C_2H_4 production over CH_4.[30] To this end, surface density thresholds have been determined, above which adsorbate interactions affected reaction mechanisms.[31] Due to its multicarbon CO_2RR products, Cu has been studied extensively through calculations to better understand density-based adsorbate interactions.[32,33] Following the logic of proximity-based adsorbate−adsorbate interactions affecting the CO_2RR mechanisms, one can also expect that adsorbate orientation could alter the electrocatalytic process. In such an instance, overall orientation is correlated with surface density at high concentrations, and orientation relative to neighboring molecules can impact the orbital overlap necessary for C−C bond formation. However, to the best of our knowledge, no published works report the orientation angles of intermediate *CO under applied potentials relative to the electrocatalyst surface.

A common experimental approach to studying Au CO_2RR is *in situ* spectroscopy of intermediates such as IR and Raman. For example, Yang et al. have compared CO_2RR on Au, Pt, and Cu surfaces, determining that C- and O-bound intermediates can result in different reaction pathways using surface-enhanced IR absorption.[34] In another example, IR experiments revealed a unique weakly bound peak for *CO on Au.[35] Moreover, Yogesh et al. showed that while adsorbed water on Au electrodes could cause *CO to be released, adsorbed CO_3^{2-} promoted its accumulation to improve the reaction.[9,18] Other work has shown that the Au surface restructures irreversibly to give an increased number of bridge sites for CO binding within the initial tens of seconds of CO_2RR.[36] Interestingly, Xu et al. systematically addressed CO_2RR and found only one CO peak at the Au surface unless a Pt counter electrode or lower-purity solutions were used.[37−42] In another study, it was shown that while surface-enhanced IR and Raman techniques give similar information about strongly adsorbed species, their weakly adsorbing sensitivities differ.[42] Furthermore, standard IR and Raman spectroscopy techniques have no surface/interfacial specificity and cannot directly probe reaction intermediates at electrode surfaces without some contribution from the bulk system.[43] While surface-enhanced Raman and IR spectroscopy techniques can possess some surface-specificity, they require specialized electrodes to be used, complicating the system.[44] To develop a robust understanding of the CO_2RR at electrode surfaces, a method with both inherent surface-specificity and *in situ* practicality is ideal.

One such interface-specific *in situ* technique is vibrational sum-frequency generation (SFG), a nonlinear optical spectroscopy.[45−48] Recently, SFG has been applied to investigate CO_2RR on Au electrode surfaces, focusing on molecular characteristics at the electrode/electrolyte interface.[29−33,49−58] For example, Wallentine et al. exploited a plasmonic resonance with a Au film to probe the Au/electrolyte interface *in situ* with SFG spectroscopy with excellent sensitivity.[51] They determined that the reaction is limited by the CO_2 adsorption rate, where upon CO production, cations adsorb to the electrode surface and hinder further reaction.[52] In another case, Rebstock et al.[53] used SFG to identify the direct adsorption of CO to inactive surface sites, showing that solvation shells of cations differed for active and inactive adsorption sites. Further use of SFG to probe CO_2RR on gold by Zhu et al. studied the interfacial electric field, revealing contributions from the Stern layer and the Onsager field, and correlated them with CO_2 activation.[59] SFG has also been used to investigate the character of the electric double layer at Au surfaces, observing opposite changes to the SFG intensity under applied bias for different electrolytes.[54] In other investigations, Huang-Fu et al. also found that only the linearly adsorbed CO was detected for Au electrodes, while ethoxy-adsorbed species were observed at Cu surfaces with no indication of a CO bond.[50] These observations led to the conclusion that the variable orientation at the Cu surface compared to Au may promote hydrocarbon formation. While these preceding works shape our understanding of CO_2RR at metal electrode surfaces,[9] the CO

https://doi.org/10.1021/jacs.5c04276
J. Am. Chem. Soc. 2025, 147, 19101−19112

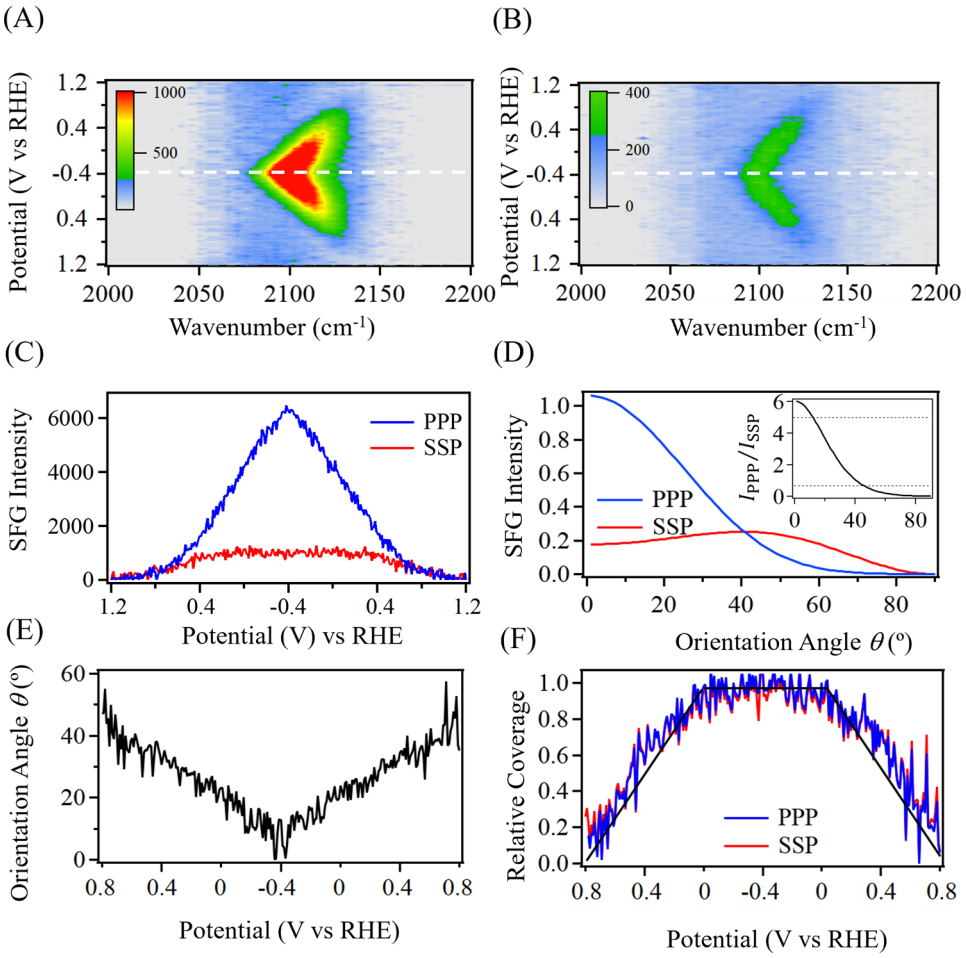

Figure 2. EC-SFG maps under PPP (A) and SSP (B) polarization combinations at the Au surface as a function of the applied potential (2 mV s^{-1} scan rate and 5 s collection time). (C) SFG intensity as a function of the applied potential from 1.2 V to −0.4 V under PPP (blue) and SSP (red) polarization combinations. (D) Simulated SFG intensities as a function of the molecular orientation under PPP (blue) and SSP (red) polarization combinations using $C_{\infty v}$ symmetry and r = 0.27; the inset shows the intensity ratio, I_{PPP}/I_{SSP}, as a function of the molecular orientation with a narrow distribution. (E) Orientation angle of *CO at the Au surface as a function of the applied potential obtained from the experimental results. (F) Relative coverage of *CO at the Au surface obtained using PPP-(blue) and SSP-(red) polarized experimental data as a function of the applied potential; black lines are to guide the eye.

orientation angle, binding energy, surface density, and production kinetics remain ambiguous.

In this work, we employed high-efficiency electrochemical SFG (EC-SFG) spectroscopy to thoroughly analyze the CO_2RR on Au electrodes to minimize assumptions and view the reaction as a whole. We conducted EC-SFG experiments *in situ* with cyclic voltammetry, providing an unprecedented time resolution of 0.2 s. This high-performance method allowed us to quantify molecular orientation through polarization-resolved SFG experiments for the first time. We also determine *CO binding energies and extract intermediate surface density. Furthermore, the time resolution allows us to examine the kinetics of the CO_2RR on Au, estimating the reaction rate. These achievements better inform electrochemical CO_2RR on metal surfaces and provide a methodological framework for better understanding electrochemical mechanisms with the goal of executing efficient clean energy production and simultaneous greenhouse remediation.

2. RESULTS

2.1. *In Situ* Identification of the *CO Intermediate of the CO_2RR on Au Surfaces. The analysis of the CO_2RR on Au electrodes using EC-SFG begins with the measurement of successive SFG spectra during the collection of cyclic voltammograms (CV), as shown in Figure 1. For clarity, the measured current density (mA cm^{-2}) is shown versus the applied potential in Figure 1A. By collecting the CV from 1.2 to −0.4 V and back to 1.2 V, we obtained cathodic and anodic current densities that align with the literature.[51,52] In Figure 1B, we present the two-dimensional (2D) pseudocolor plot obtained from these experiments with wavenumber (cm^{-1}) on the *x*-axis, applied potential (V *vs* RHE) on the *y*-axis, and SFG intensity on the *z*-axis (color bar). By monitoring the SFG spectra during the potential sweeps, we observed both changes in intensity and frequency: intensity begins to increase at potentials <0.6 V, reaching a maximum at −0.4 V and decreasing over the reverse sweep. Figure 1C shows representative spectra with applied potentials. From the individual spectra, the cyclic changes in both intensity and frequency are explicit. To precisely monitor the spectral shift with applied potentials, we compared the central SFG peak frequency with the applied potential, as shown in Figure 1D. Here, we see that the peak shifts linearly from 2124.2 cm^{-1} at 0.8 V to 2097.6 cm^{-1} at −0.4 V. Accordingly, this SFG peak

https://doi.org/10.1021/jacs.5c04276
J. Am. Chem. Soc. 2025, 147, 19101−19112

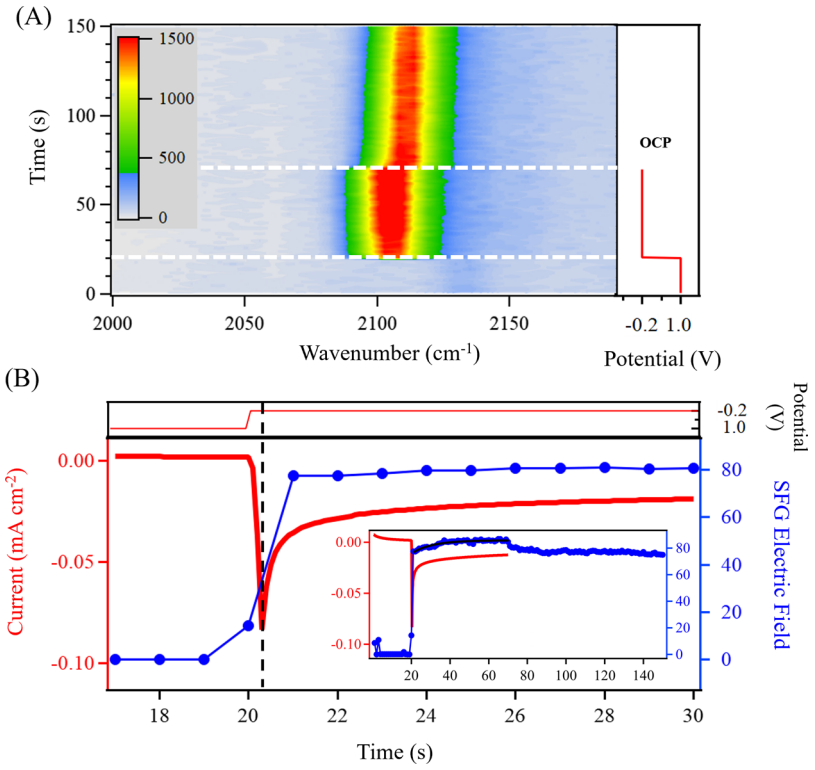

Figure 3. Time-dependent EC-SFG data of *CO generation and diffusion under PPP polarization and variable applied potential: 1.0 V for 20 s to clean the surface and then set at −0.2 V to generate *CO for 50 s, followed by an open-circuit potential (OCP) for 80 s. (A) 2D EC-SFG map over a 150 s span showing cleaning, generation, and diffusion and exhibiting changes in intensity and spectral frequency. (B) Early 13 s time window of current density (red, left) and SFG electric field (right, blue). The top panel shows applied potential. The inset shows the full time window of the three-step process.

was assigned to the *CO intermediate state, where the asterisk indicates that the molecule is bound to the surface.[51−53,59] This shift in peak frequency is a result of the Stark effect, and the increase in spectral intensity may be the result of an increased *CO surface population combined with a more ordered and upright molecular orientation. With the change in peak position being nearly mirrored on the cathodic and anodic sweeps, we obtained Stark shift values of 24.6 and 25.2 cm^{-1} V^{-1} by fitting (red line), respectively, which are in the range of reported values.[50,59]

The most outstanding property of our high-performance EC-SFG setup is the high signal intensity, which provides multiple advantages over previous SFG experiments that were interfaced with electrochemical measurements. First, the signal intensity allowed us to run our EC cycles at fast scan rates without loss of information, as shown in Figure S2, where EC-SFG spectra were collected at scan rates from 10 to 100 mV s^{-1} and provided comparable results. This allowed us to use a minimum acquisition time of 0.2 s and thereby provide meaningful time resolution to kinetics experiments, much faster than previous reports with acquisitions on the order of tens of seconds.[50−53,59] Additionally, this sampling time could be readily improved up to 10 ms, or less, by using a CCD detector with a faster sampling time (for example, 1 MHz). Second, this unprecedented signal intensity allowed us to obtain EC-SFG spectra in the SSP polarization combination, in addition to the typical PPP configuration. Previous EC-SFG works on pure Au surfaces only reported the PPP polarization combination since it is more intense, where SSP spectra of *CO were not obtainable.[50−54,59] By obtaining both PPP and SSP polarization combination spectra, we can compare them and extract molecular orientational information about *CO adsorbed on Au electrode surfaces,[47,60] a parameter that has the potential to affect reaction product yield distribution due to surface density and orbital overlap.

2.2. Polarization-Dependent SFG Experiments. To determine the orientation angle of the generated *CO intermediate species, we collected EC-SFG spectra at PPP and SSP polarization combinations,[47,60] as shown in Figure 2A,B, respectively. Both polarization combinations exhibit a Stark shift similar to that described above. However, the intensity of the two polarization combinations is dynamic with applied potential, as shown in Figure 2C. Here, we see that at −0.4 V, the peak potential for both experiments, the PPP polarization is much greater in intensity than SSP and, at more positive potentials, the PPP intensity is overtaken by SSP polarization combination. To use these data to quantify the *CO orientation angle, we simulated the relative intensities of the polarized SFG response from the $C_{\infty v}$-symmetric *CO group at different orientation angles relative to the surface normal using the molecular hyperpolarizability ratio, r = 0.27,[61,62] as shown in Figure 2D. A detailed description of the simulations is found in the Supporting Information (SI). The inset explicitly shows the intensity ratio, I_{PPP}/I_{SSP}, as a function of the orientation angle.[47] These simulations show that at more vertical orientations, the PPP polarization combination should be much more intense than the SSP, while at flatter orientation angles, the opposite ratio should be observed. From these data, we then extracted the orientation angle of the produced *CO intermediate relative to the surface normal of the Au electrode,

https://doi.org/10.1021/jacs.5c04276
J. Am. Chem. Soc. 2025, 147, 19101−19112

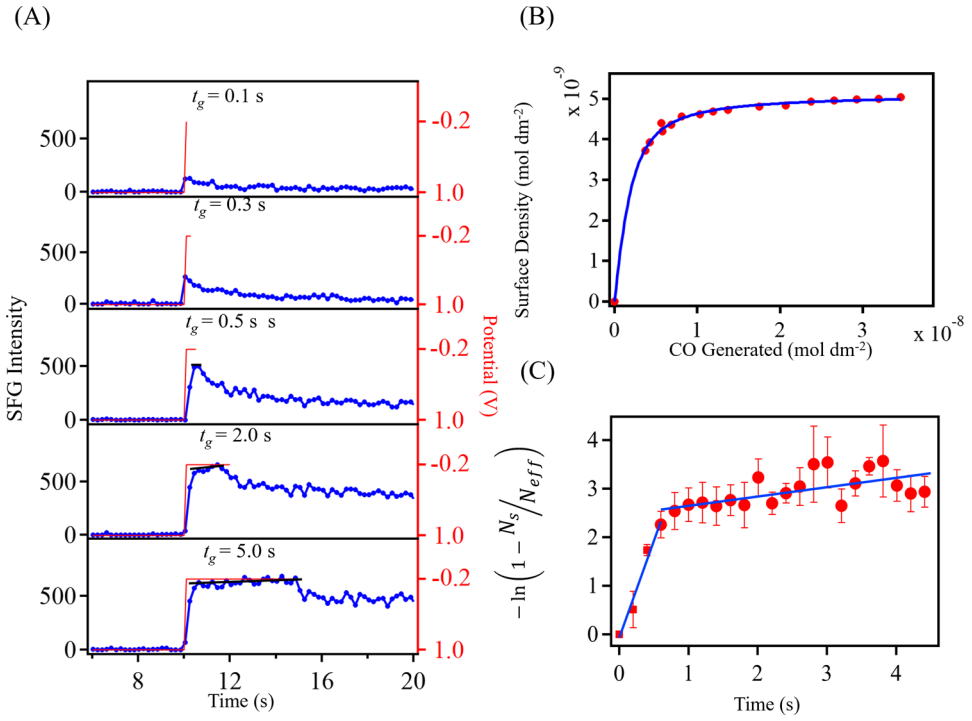

Figure 4. (A) EC-SFG intensity over time for different *CO generation times (t_g = 0.1−5.0 s) with representative measured potentials over time shown in red. (B) Surface density (mol dm^{-2}) of *CO as a function of the overall produced concentration. Red dots represent experimental data, and the blue line is a curve fitting to eq 3. (C) $\ln(1 - N_s/N_{eff})$ over time at averaged t_g from 1.0 to 5.0 s; red dots indicate experimental data, error bars represent the experimental standard deviation, and the blue line is a curve fitting to a linear equation.

as shown in Figure 2E. These results show a great change in orientation over the applied potential range, where the *CO has an angle of 45.0 ± 1.7° at 0.8 V and then stands nearly upright with an angle of 8.3 ± 1.7° at −0.4 V. Additionally, there is an interplay between the CO surface density and orientation, where a more upright configuration can allow closer packing of adsorbates. We then used this relationship to produce Figure 2F, which compares the relative surface density (100% occupation) as a function of the applied potential. Here, we see that surface density increases linearly with decreasing applied potential from 0.8 to 0.0 V and then forms a plateau from 0.0 to −0.4 V, at which point the cycle repeats in reverse and is relatively symmetric. From this analysis, we estimated that the maximum density is reached near the 0.0 V (20.2 ± 1.7°) applied potential and does not meaningfully increase with more negative potential application. These results corroborate our hypothesis that the highest EC-SFG intensity is correlated to greater interfacial ordering and density, suggesting that the orientation may not be affected by molecular packing and *vice versa* at the present surface densities.

2.3. Time-Resolved EC-SFG on Au Surfaces. The kinetics of the CO_2RR on Au electrodes was next investigated, where the high-performance nature endowed meaningful time resolution to EC-SFG experiments for the first time. These time-resolved experiments were conducted by collecting SFG spectra from the Au/electrolyte interface every 0.9 s while applying a potential of 1.0 V for 20 s to remove and clean-bound *CO, followed by −0.2 V for 50 s to generate *CO, and then with no applied potential (open-circuit potential (OCP)) for the remaining 80 s, as shown in Figure 3A. Here, no considerable SFG signal is observed during the electrode cleaning step. This was followed by a sharp increase upon application of −0.2 V, showing the *CO peak at 2102.9 cm^{-1}, which gradually increased toward a plateau over the applied potential time. Interestingly, once the potential was no longer being applied, we observed a slight red shift to 2113.5 cm^{-1} accompanied by a decrease in signal intensity. Over the subsequent waiting time, the SFG response remained consistent.

To better understand the kinetics of the *CO generation process, we compared the time traces for the SFG electric field, $E_{SFG}(t)$, and the measured current density, $I(t)$, from this experiment in Figure 3B. Here, the SFG electric field is proportional to the surface density, $N_s(t)$, and the measured current density is related to not only the surface density but also the bulk density, $N_\infty(t)$, and the thickness of a diffusion layer, $\delta(t)$: $I(t) \propto N_s(t) - N_\infty(t)/\delta(t)$. Likewise, $E_{SFG}(t) \propto N_s(t)$. As shown in the figure, both current density and SFG responses are at zero during the first 20 s cleaning period, 1.0 V. Upon changing the potential to −0.2 V (t = 20.1 s), we see the current density begin to decrease rapidly, reaching −0.12 mA cm^{-2} at t = 20.3 s. Most notably, there is an increase in the EC-SFG electric field, which is nearly instantaneous at t = 20 s. Over the course of the next second, the EC-SFG field, and thereby $N_0(t)$, reaches a local maximum, while the current density is only at ∼70% of its local maximum. As the subsequent 9 s are observed, the EC-SFG electric field is nearly constant, only increasing a few percent, while $I(t)$ slowly approaches a plateau. As shown in the inset, the $I(t)$ and $E_{SFG}(t)$ approach similar slopes on a larger time scale, while were not coincident at short times. This is because while the SFG intensity is directly proportional to the number of adsorbed *CO, the current density must also account for CO in the bulk and diffusion layer. After the potential is no longer being applied, there is a small decrease in $E_{SFG}(t)$ since new

https://doi.org/10.1021/jacs.5c04276
J. Am. Chem. Soc. 2025, 147, 19101−19112

*CO molecules are not being generated and stay relatively constant due to the already adsorbed *CO. This decrease in intensity may also be the result of a change in molecular orientation once the system returns to the OCP. These results demonstrate the importance of having sufficient time resolution with EC-SFG experiments to obtain a more detailed perspective on the electrocatalytic processes at the surface.

The surface density of *CO, another crucial factor in the CO_2RR at electrode surfaces, was next investigated by making electrochemical SFG measurements with varying times of applied potential. A minimum acquisition time of 0.2 s was used for these kinetic experiments of 0.2 s. By doing so, we can form a relationship with the total *CO generated over time using the SFG intensity. As shown in Figure 4A, the 10 s cleaning step at 1.0 V was performed, followed by applying a potential of −0.2 V for increasing lengths of time defined as generation time, t_g. At low t_g, 0.1−0.3 s, we see that the generation time is not long enough to reach the maximum SFG intensity. On the other hand, a longer t_g, at least 0.5 s, we see that the SFG intensity reaches a nearly stable value and starts to gradually increase, as noted above. Additionally, the SFG intensity after the applied potential was stopped tended to return to a lower value faster for a shorter t_g and then remained stable. This is indicative of a larger proportion of CO desorbing with time since less was produced for shorter t_g values.

These data were then used to determine the surface density and total *CO produced, which can be used to quantify the kinetics and thermodynamics that govern the generation and desorption processes. The surface density, Θ, is defined as the ratio of *CO, N_s, to the number of *CO molecules to fulfill a totally covered surface, N_{max}. Since the input of two electrons is required to generate the *CO species and the current is known, we can then estimate the concentration of *CO in mol dm^{-2}. The *CO surface density and the total intermediate produced were corrected for desorption by including the desorption rate constant, k_d, of 0.25 s^{-1}, as shown in the SI, to account for reaction products moving away from the electrode and no longer contributing to the SFG signal. As shown in the SI, we found that at our maximum SFG electric field obtained by applying a potential of −0.2 V represents a surface density of 5.04×10^{-9} mol dm^{-2} (3.03×10^{13} molecules cm^{-2}). The surface density was calculated for each generation time, t_g, as shown in the SI. This then allowed us to determine the surface density as a function of generated CO, as shown in Figure 4B. This isotherm appears to exhibit a typical Langmuir trend and begins to plateau at *CO concentrations greater than ~8.13×10^{-9} mol dm^{-2}, indicating the point at which maximum surface density was achieved.

While this isotherm can inform us about the thermodynamics of the CO_2RR on Au electrodes, we can also use this information to investigate the reaction kinetics. Since the CO_2RR proceeds as a first-order reaction, we can use the following relationship to determine the rate constant:[36]

$$E_{SFG} \propto N_s \propto N_{eff}(1 - e^{-k_g t}) \quad (1)$$

where N_{eff} is the effective number of reaction sites and k_g is the generation rate constant. As such,

$$-\ln\left(1 - \frac{N_s}{N_{eff}}\right) = k_g t \quad (2)$$

This procedure allowed us to obtain the right side of eq 2 as a function of time. We plotted $-\ln(1 - N_s/N_{eff})$ over time to extract the rate constant, as discussed in the following. As shown in Figure 4(C), $-\ln(1 - N_s/N_{eff})$ increases linearly for the segment of time <1 s and then proceeds more slowely. The results from using different generation times were averaged, showing that it did not significantly affect the reaction rate, and all t_g values tested exhibited the same two-stage progression. In addition, we have made a full analysis of rates for the generation, desorption, and resorption in the Supporting Information. The rate constant for the desorption was found to be 0.25 s^{-1}, while the rate constant for the readsorption varied from 0.0195 to 0.469 s^{-1}. These kinetic results allow us to reveal the reaction rate of the intermediate during the CO_2RR.

3. DISCUSSION AND CONCLUSIONS

We have shown that *in situ* EC-SFG spectroscopy can provide comprehensive analyses of the CO_2RR on Au electrodes and can now combine these results to uncover the governing chemistry of the system. There are three central metrics that govern the thermodynamics of the CO_2RR on electrode surfaces: molecular orientation, intermolecular distance, and surface binding energies. Starting with orientation, the angle of adsorbed molecules—reactants, intermediates, or products—with respect to the surface normal impacts the alignment of their molecular orbitals relative to each other and can therefore impact reaction products and pathways.[3,12,27,63] These high-performance EC-SFG experiments also allowed *in situ* quantification of *CO concentration at Au electrodes for the first time, contributing to the metrics of surface density and binding energy. We can now combine all three of these metrics in a self-consistent manner, which minimizes assumptions. Additionally, the reaction rate of the CO_2RR, or the speed at which it proceeds, is an important metric that is not only indicative of its efficiency but is also very useful for comparing different electrocatalyst systems.[64−67] Here, we use our results to discuss these thermodynamic and kinetic characteristics of the CO_2RR on Au electrodes.

3.1. Thermodynamics of the CO_2RR on Au Electrode Surfaces.

A commonly studied property of catalytic surfaces is their binding energy. The binding energy of the adsorbed *CO to the gold surfaces can dictate the efficiency and reaction products by affecting how tightly the two are bound together.[63,68−72] Considering the competition between the CO and CO_2, we can also consider the binding energy as an approximation index to assess the CO_2RR. If the binding energy is strong, more energy is required to remove *CO from the surface, which may provide more opportunities for different reactions to take place while it is immobile. On the other hand, weaker-binding energy systems require less energy to remove the adsorbed molecule from the surface, which can prematurely release, but also provide a new adsorption site for the next molecules to be reacted. As such, a balanced binding energy is necessary for the most efficient CO_2RR such that the adsorbed *CO is held tightly enough to react as needed but is also readily released to promote product turnover. To assess the binding energy of the *CO intermediate at Au electrode surfaces, we look at the SFG response as a function of the *CO concentration. First, the SFG electric field, E_{SFG}, is proportional to the number density of adsorbed molecules at the investigated interface, N_s. We can then use the Langmuir adsorption model, as described in detail in SI, to describe the *CO generation process on the gold electrode surface. The

https://doi.org/10.1021/jacs.5c04276
J. Am. Chem. Soc. 2025, 147, 19101−19112

Langmuir adsorption model describes the adsorption and desorption of molecules to a surface at equilibrium.[73] At equilibrium, we then obtain that the absolute surface density, Θ, takes the form of

$$\Theta = \frac{N_s}{N_{max}} = \frac{(C + N_{max} + 14.55/K) - \sqrt{(C + N_{max} + 14.55/K)^2 - 4CN_{max}}}{2N_{max}} \quad (3)$$

where C is the overall CO concentration, 14.55 is the density of water molecules adsorbed on the surface (mol dm^{-2}), $K = k_1/k_{-1}$, and k_{-1} is the desorption rate constant. This expression is known as the modified Langmuir equation since it accounts for the case in which $N_S \ll C$ fails. In our case, there is no *CO in the system until the appropriate potential is applied, after which it must then diffuse into the solution. This expression fits well in the *CO adsorption isotherms shown in Figure 4B. We can then extract K from the fitting and use it to calculate the binding free energy, ΔG_{*CO}, where

$$\Delta G_{*CO} = -RT \ln K \quad (4)$$

with R being the ideal gas constant (1.987×10^{-3} kcal K^{-1} mol^{-1}) and T being the temperature (295.15 K). Our experiments resulted in $\Delta G_{*CO} = -13.81 \pm 0.12$ kcal mol^{-1} (-57.78 ± 0.50 kJ mol^{-1}). Experimental reports of the *CO binding energy for the air/Au interface range between −11 and −14 kcal mol^{-1},[74−78] which aligned with appropriate density functional theory (DFT) simulation results.[79−84] The importance of ΔG_{*CO} in an electrochemical environment has been realized and investigated at the water/Au interface to understand CO_2RR process.[9,42,85] Specifically, Yogesh's group determined ΔG_{CO} of free CO on Au surfaces resulting in −14.0 kJ mol^{-1},[9] which is notably smaller than our results but was for the system of free CO adsorption. Not only did we quantify the adsorption free energy in our experiments, but the excellent time resolution afforded by our EC-SFG experiments allowed us to accurately determine the total amount of generated CO to compute high-quality isotherms. This same process can be easily extended to other systems, thereby providing necessary comparisons to correlate binding energy and reaction product distribution for different electrocatalyst systems. Furthermore, our high-performance EC-SFG experiments provide microscopic details about the structure of adsorbed *CO on electrode surfaces.

While SFG experiments have been used to probe CO orientation at electrode surfaces previously,[61,86−88] the high-performance EC-SFG system allows us to analyze the orientation of the generated *CO intermediate and its change in real time throughout the electrochemical process. As shown in Figure 2E, we observed a large change in adsorbed *CO orientation relative to the surface normal under applied potential, starting at an angle of 45.0 ± 1.7° at 0.8 V and changing to 8.3 ± 1.7° at −0.4 V. This indicates that while a range of applied potentials can generate the *CO intermediate, different potential values may impact overall reaction products and mechanisms due to the dynamic configurational behaviors of the intermediate in the CO_2RR process.

To thoroughly examine the exciting orientational analysis afforded by our high-performance EC-SFG experiments, we consider two central questions: (1) How can we be confident in the precision of our orientation analysis when using a manually polished polycrystalline electrode? and (2) if these orientational results are precise and accurate, what are the driving forces behind their change with applied potential? First, the perspective of the laser spot on the Au electrode surface is considerably more macroscopic than that of an individual *CO at an active site. Given the effective irradiated area, the measured orientational angle is the average of more than 10^9 *CO species for a fully covered surface. Such an ensemble average effectively absorbs intricacies in adsorbate orientation, which can result from surface nanostructure due to polishing a polycrystalline electrode as opposed to using an atomically flat single crystal. Along these lines, any potential-dependent surface restructuring is also absorbed by the ensemble average approach: *i.e.*, the EC-SFG methodology cannot distinguish changes in *CO orientation as the result of restructuring or purely due to applied potential because it does not measure potential-dependent restructuring. Nevertheless, this does not detract from the significance of the results or the EC-SFG investigation, as investigations of more well-defined single-crystalline electrode surfaces are disconnected from the readily accessible polycrystalline electrodes used in practical applications. Second, the driving force for the potential-dependent *CO orientation change is a combination of the potential-dependent initial CO_2 adsorption configuration and the thermodynamic drive from the applied overpotential. It is noted that the commonly accepted normal orientation of the *CO on Au surfaces is observed here, but at more negative potentials, and we do not intend to discount such previous conclusions, but to highlight that EC-SFG measurements can discern changes in the orientation angle with applied potential. The measured orientation angle of the *CO intermediate is directly related to the orientation of the initially absorbed CO_2 molecule since it is measured after the removal of OH^- and before the final product can become reoriented. Thus, since the CO_2 orientation varies with applied potential, the angle of the intermediate will follow. The applied overpotential also provides more energy to the system, which results in a greater influence over the adsorbate and thereby produces a more ordered and vertical intermediate. An interesting follow-up to these possible mechanisms would be to quantify the orientation of the initial CO_2 adsorbate to determine the interplay between the applied potential's influence on the *CO orientation directly and indirectly.

The effect of surface density on the CO_2RR mechanism and therefore products is simple: adsorbed *CO molecules must be close enough to interact with each other to form multicarbon compounds, but not too close as to restrict interactions between adsorbates and other solute species.[31−33] For this reason, we used our high-performance EC-SFG technique to estimate the surface density of the *CO intermediate. First, the production of the *CO intermediate adsorbed onto the Au electrode surface occurs by reacting CO_2 with water and two electrons to produce the CO species and two hydroxides.[16] Since current density is proportional to charge, we can then use our electrochemical SFG measurements to determine the surface density of *CO, as detailed in the SI. Briefly, it was found that the plateau in the SFG electric field corresponds to an occupation of 100% of the effective surface sites. By dividing by the surface area, we found that the surface density of the *CO intermediate is 5.04×10^{-9} mol dm^{-2} (3.03×10^{13} molecules cm^{-2}). As shown in the SI, this is only about 4.2% of the total density possible for *CO adsorbed to the gold surfaces.[75] As such, these sparsely spaced species are unaffected by neighboring molecules, suggesting that the measured

https://doi.org/10.1021/jacs.5c04276
J. Am. Chem. Soc. 2025, 147, 19101−19112

molecular orientation is more directly a function of the applied potential rather than molecular packing. If the more vertical orientation was the result of molecular packing, we would expect to see its onset coincident with maximum surface density; instead, as shown in Figure 2E,F, molecular orientation keeps approaching the surface normal at potentials beyond which surface density has been maximized. Furthermore, the distance between adjacent *CO molecules is large such that intermolecular interactions are unlikely, which aligns with the fact that CO gas is the main product. If the intermolecular distance was smaller, we would expect to see an evolution of other reaction products, possibly with C−C bonds, as is the case with Cu electrodes,[89−95] as long as the binding energy and molecular orientation are commiserated with such reactions. Along these lines, the importance of intermediate convergence cannot be neglected in understanding the reaction pathways and mechanism in the CO_2RR, as all three criteria are necessary to thoroughly characterize a given electrocatalytic system.

Under electrochemical conditions, we determined that the surface coverage of CO on Au is approximately 4.2%, which is markedly lower than that observed at the air−metal interface. While this observation agrees with previously reported studies,[53] the underlying factors responsible for such low coverage merit further investigation. There are several possible explanations for this observation. (1) Competition with the hydrogen evolution reaction (HER) may lead to active sites being occupied by H atoms or H_2 molecules.[4,15,17,18,96−98] The local concentration of CO_2 near the electrode is difficult to sustain.[16,98,99] (2) Local pH variations at the electrode/electrolyte interface and the OH− block active sites or react with the CO_2. According to the CO_2RR equation, $CO_2 + H_2O + 2e^- \rightarrow 2OH^- + CO$, the local concentration of OH− increased as the reaction proceeds.[16,99−101] (3) Mass transport limitations of CO_2 during prolonged electrolysis, apart from the geometric configuration of the instrument, factors discussed in (1) and (2), also limit the access of CO_2 to the surface of the Au electrode. The generated *CO absorbed at the Au surface also blocks the active site for CO_2. While the complexity of the actual CO_2RR process at Au surfaces is apparent, the EC-SFG experiments presented here can provide more information to better understand the system. Recently, phase-resolved second-harmonic generation spectroscopy was used to investigate absolute orientation and number density during water flipping in the Stern layer during the oxygen evolution reaction (OER).[103] Such a scheme can also be introduced to EC-SFG experiments in the future to provide additional information during OER, CO_2RR, and other important electrochemical processes.[102]

Taken together, the binding energy, absolute surface density, and orientation angle of an intermediate should be fully considered in understanding its thermodynamic behaviors in the CO_2RR: (1) The binding energy of a molecule can affect its catalytic residence time and reaction rate, which impact both product distribution and reaction kinetics. (2) Adsorbate surface density affects adsorbate−adsorbate interactions and their couplings, thereby impacting product distribution. (3) Adsorbate orientation affects precise adsorbate−adsorbate interactions and can be associated with surface density in a codependent relationship. To best understand these processes and how they are intertwined, further comprehensive investigations, such as that presented there, conducted on different electrocatalyst systems are necessary and should be supported by complementary computations, such as those that may test correlations between intermolecular interactions and binding energy. By systematically conducting similar experiments to those presented here with electrocatalysts that produce more complex CO_2RR products, most robust correlations can be made between the thermodynamics of the process and the product yield distribution.

3.2. Reaction Rates of the CO_2RR on Au Electrode Surfaces. The two essential concepts that govern the CO_2RR on Au electrodes are the thermodynamics and kinetics of the reaction. While the thermodynamic parameters discussed above describe the favorability and thereby the probability that a process will occur, the kinetics of the process describe the speed at which it can and does proceed. By fitting the $-\ln(1 - N_s/N_{eff})$ data to a linear equation in Figure 4C, k_1 corresponds to the slope of the line, which was determined to be about $3.98 \pm 0.49\ s^{-1}$ at $t < 1.0$ s and $0.19 \pm 0.05\ s^{-1}$ at longer reaction times. As such, the electrocatalytic reaction occurs faster at earlier times and slower after it has progressed for >1 s. This is due to the limited active *CO binding sites that block new CO_2 molecules from adsorbing to be reduced and is a function of ΔG_{*CO}. A possible cause for this reduction in rate at longer generation times is geometry-restricted diffusion due to the EC cell, which was used. The thin layer of electrolyte between the window and electrode significantly reduces the available electrolyte volume to bring in new CO_2 or remove produced CO. However, if the produced CO were readsorbed, we would expect to see asymmetry between the cathodic and anodic sweeps in the EC-SFG measurements. However, the EC-SFG maps in Figures 1 and 2 show symmetric signals for the sweeps. For these reasons, we emphasize that the rate constant should be determined for the short generation times <1 s. Hence, a rate constant of $3.98\ s^{-1}$ is the most accurate estimate of the true value that can be gleaned from our experiments. Due to our experimental geometry, such a setup is not ideal for long-term kinetics analyses.

While the reaction rate constant can be viewed as a measure of quality for gold electrodes performing the CO_2RR, another way to look at the rate of the process is through the turnover frequency (TOF),[64−66,103] which has the same units as the rate constant: s^{-1}. As its name implies, the TOF is a measure of successful catalytic turnovers ($CO_2 \rightarrow CO$)[65] and is defined as the time derivative of the number of turnovers. The reaction rate constant calculated above is more appropriate than the commonly used TOF for our CO_2RR on the Au system since the absolute number of effective sites is not known. The reaction rate constant is an important metric by which we can assess a material's fitness for electrocatalytic processes. Additionally, there is a correlation between how tightly adsorbates are bound and the reaction rate. Thus, tightly bound adsorbates, which are necessary for producing further reduced carbon products, can result in a slower reaction at the cost of producing the desired products.

We believe that this work contains the necessary first steps for better understanding the reaction and how other catalytic systems may promote its product distribution. One such system is the catalytic CO_2RR on Cu electrode surfaces. Specifically, the pathway of the CO_2RR on Cu surface is heavily dependent on the *CO surface density, as it affects C_{2+} production by promoting the C−C coupling.[89] This was demonstrated by observing an increase in FE of C_2H_4 by increasing the *CO surface density.[10,89,91,94,95,104,105] In the

https://doi.org/10.1021/jacs.5c04276
J. Am. Chem. Soc. 2025, 147, 19101−19112

meanwhile, a higher *CO surface density, Θ, leads to a lower surface density of adsorbed water molecules capable of donating protons, which could lower the reaction order of CO to suppress HER.[93] However, the *CO surface density at Cu surfaces has not been experimentally quantified. In addition to surface density, measuring the binding free energy of the intermediate and final products is helpful in the determination of a mechanism for any electrochemical reaction. For example, calculating the ΔG of *H−CO, *CHO, *CH_2CHO, and *CH_3CH_2O for the CO_2RR on Cu surfaces would elucidate the roles of the different intermediates and their binding strength with Cu.[28,106,107] Recently, much focus has been devoted to the calculation of ΔG to try to understand the dynamic behavior of CO_2,[70] CO,[63,71,72,108−110] and H_2O[111,112] at the electrode surfaces and how they affect reaction pathways.[68,69] However, most studies revolve around the air/Cu surface instead of an electrochemical environment and are lacking experimental support. Our EC-SFG technique can provide valuable insight into the CO_2RR on Cu electrodes by quantifying binding energy and looking at the system and others comprehensively.

4. SUMMARY

In this work, we demonstrated the ability of high-efficiency electrochemical sum-frequency generation (EC-SFG) spectroscopy to extract vital thermodynamic and kinetic information about the electrochemical CO_2 reduction reaction (CO_2RR) *in situ*. These experiments provided high-intensity SFG responses, allowing us to quantify the orientation of the surface-bound *CO intermediate to range between 8.3 and 45.0° with respect to the surface normal with applied potential for the first time. These experimental results were then used to determine a maximum surface density of 5.04×10^{-9} mol dm^{-2} (3.03×10^{13} molecules cm^{-2}) with relative coverage of *ca.* 4.2% and a binding free energy of −13.81 kcal mol^{-1} (57.78 kJ mol^{-1}) with minimal assumptions. Correlations between surface density and orientation showed that *CO in our case is not tightly packed enough to affect their interfacial orientation, with orientation primarily hinging on applied potential. Our results have demonstrated that the binding free energy, orientation angle, and absolute surface density of an intermediate together are complete descriptors for understanding its thermodynamic behaviors in the CO_2RR on metal surfaces. Furthermore, the experimental setup afforded fast time resolutions on the scale of hundreds of milliseconds, which allowed us to calculate the reaction rate constant for the production of *CO to be about 3.98 s^{-1}. This work not only demonstrated the potential of high-efficiency EC-SFG spectroscopy to provide an all-inclusive analysis of the CO_2RR on metal surfaces but also opened the door for other catalysts to be investigated using the technique to determine the best system for efficient CO_2RR.

■ ASSOCIATED CONTENT

Supporting Information

The Supporting Information is available free of charge at https://pubs.acs.org/doi/10.1021/jacs.5c04276.

Schematic of the EC-SFG experimental setup; EC-SFG spectra under different potential scan rates; orientational analysis from EC-SFG spectra; analysis of rates for generation, desorption, and readsorption; and determining surface density and free energy of *CO (PDF)

■ AUTHOR INFORMATION

Corresponding Authors

Zhi-Chao Huang-Fu − *Department of Chemistry and Biochemistry, Utah State University, Logan, Utah 84322, United States*; Email: zhichao.huangfu@usu.edu

Yi Rao − *Department of Chemistry and Biochemistry, Utah State University, Logan, Utah 84322, United States*; orcid.org/0000-0001-9882-1314; Email: yi.rao@usu.edu

Authors

Hui Wang − *Department of Chemistry and Biochemistry, Utah State University, Logan, Utah 84322, United States*

Haley Fisher − *Department of Chemistry and Biochemistry, Utah State University, Logan, Utah 84322, United States*

Jesse B. Brown − *Department of Chemistry and Biochemistry, Utah State University, Logan, Utah 84322, United States*

Tong Zhang − *Department of Chemistry and Biochemistry, Utah State University, Logan, Utah 84322, United States*

Fuzhan Song − *Department of Chemistry and Biochemistry, Utah State University, Logan, Utah 84322, United States*

Yuqin Qian − *Department of Chemistry and Biochemistry, Utah State University, Logan, Utah 84322, United States*

Complete contact information is available at: https://pubs.acs.org/10.1021/jacs.5c04276

Notes

The authors declare no competing financial interest.

■ ACKNOWLEDGMENTS

This material is based upon work supported by the National Science Foundation under Grant No. 2045084.

■ REFERENCES

(1) Alsos, I. G.; Ehrich, D.; Thuiller, W.; et al. Genetic consequences of climate change for northern plants. *Proc. R. Soc. B* **2012**, *279* (1735), 2042−2051.

(2) Nitopi, S.; Bertheussen, E.; Scott, S. B.; et al. Progress and Perspectives of Electrochemical CO_2 Reduction on Copper in Aqueous Electrolyte. *Chem. Rev.* **2019**, *119* (12), 7610−7672.

(3) Ma, Y.; Wang, J.; Yu, J.; et al. Surface modification of metal materials for high-performance electrocatalytic carbon dioxide reduction. *Matter* **2021**, *4* (3), 888−926.

(4) Jovanov, Z. P.; Hansen, H. A.; Varela, A. S.; et al. Opportunities and challenges in the electrocatalysis of CO_2 and CO reduction using bifunctional surfaces: A theoretical and experimental study of Au−Cd alloys. *J. Catal.* **2016**, *343*, 215−231.

(5) Goyal, A.; Marcandalli, G.; Mints, V. A.; Koper, M. T. M. Competition between CO_2 Reduction and Hydrogen Evolution on a Gold Electrode under Well-Defined Mass Transport Conditions. *J. Am. Chem. Soc.* **2020**, *142* (9), 4154−4161.

(6) White, J. L.; Baruch, M. F.; Pander, J. E.; et al. Light-Driven Heterogeneous Reduction of Carbon Dioxide: Photocatalysts and Photoelectrodes. *Chem. Rev.* **2015**, *115* (23), 12888−12935.

(7) Kuhl, K. P.; Hatsukade, T.; Cave, E. R.; Abram, D. N.; Kibsgaard, J.; Jaramillo, T. F. Electrocatalytic Conversion of Carbon Dioxide to Methane and Methanol on Transition Metal Surfaces. *J. Am. Chem. Soc.* **2014**, *136* (40), 14107−14113.

(8) Hadjiivanov, K. I.; Vayssilov, G. N. Characterization of oxide surfaces and zeolites by carbon monoxide as an IR probe molecule. *Adv. Catal.* **2002**, *47*, 307−511.

(9) Wuttig, A.; Ryu, J.; Surendranath, Y. Electrolyte Competition Controls Surface Binding of CO Intermediates to CO_2 Reduction Catalysts. *J. Phys. Chem. C* **2021**, *125* (31), 17042−17050.

(10) Kuhl, K. P.; Cave, E. R.; Abram, D. N.; Jaramillo, T. F. New insights into the electrochemical reduction of carbon dioxide on metallic copper surfaces. *Energy Environ. Sci.* **2012**, *5* (5), 7050−7059.
(11) Jiang, T.; Mowbray, D. J.; Dobrin, S.; Falsig, H.; Hvolbæk, B.; Bligaard, T.; Nørskov, J. K. Trends in CO Oxidation Rates for Metal Nanoparticles and Close-Packed, Stepped, and Kinked Surfaces. *J. Phys. Chem. C* **2009**, *113* (24), 10548−10553.
(12) Kortlever, R.; Shen, J.; Schouten, K. J. P.; Calle-Vallejo, F.; Koper, M. T. M. Catalysts and Reaction Pathways for the Electrochemical Reduction of Carbon Dioxide. *J. Phys. Chem. Lett.* **2015**, *6* (20), 4073−4082.
(13) Wang, Y.; Liu, J.; Wang, Y.; Al-Enizi, A. M.; Zheng, G. Tuning of CO_2 Reduction Selectivity on Metal Electrocatalysts. *Small* **2017**, *13* (43), No. 1701809.
(14) Pawar, A. U.; Kim, C. W.; Nguyen-Le, M.-T.; Kang, Y. S. General Review on the Components and Parameters of Photoelectrochemical System for CO_2 Reduction with in Situ Analysis. *ACS Sustainable Chem. Eng.* **2019**, *7* (8), 7431−7455.
(15) Monteiro, M. C. O.; Philips, M. F.; Schouten, K. J. P.; Koper, M. T. M. Efficiency and selectivity of CO_2 reduction to CO on gold gas diffusion electrodes in acidic media. *Nat. Commun.* **2021**, *12* (1), No. 4943.
(16) Marcandalli, G.; Goyal, A.; Koper, M. T. M. Electrolyte Effects on the Faradaic Efficiency of CO_2 Reduction to CO on a Gold Electrode. *ACS Catal.* **2021**, *11* (9), 4936−4945.
(17) Cave, E. R.; Montoya, J. H.; Kuhl, K. P.; et al. Electrochemical CO_2 reduction on Au surfaces: mechanistic aspects regarding the formation of major and minor products. *Phys. Chem. Chem. Phys.* **2017**, *19* (24), 15856−15863.
(18) Wuttig, A.; Yaguchi, M.; Motobayashi, K.; Osawa, M.; Surendranath, Y. Inhibited proton transfer enhances Au-catalyzed CO_2-to-fuels selectivity. *Proc. Natl. Acad. Sci. U.S.A.* **2016**, *113* (32), E4585−E4593.
(19) Anfuso, C. L.; Ricks, A. M.; Rodríguez-Córdoba, W.; Lian, T. Ultrafast Vibrational Relaxation Dynamics of a Rhenium Bipyridyl CO_2−Reduction Catalyst at a Au Electrode Surface Probed by Time-Resolved Vibrational Sum Frequency Generation Spectroscopy. *J. Phys. Chem. C* **2012**, *116* (50), 26377−26384.
(20) Blizanac, B. B.; Arenz, M.; Ross, P. N.; Marković, N. M. Surface Electrochemistry of CO on Reconstructed Gold Single Crystal Surfaces Studied by Infrared Reflection Absorption Spectroscopy and Rotating Disk Electrode. *J. Am. Chem. Soc.* **2004**, *126* (32), 10130−10141.
(21) Wu, D.-Y.; Li, J.-F.; Ren, B.; Tian, Z.-Q. Electrochemical surface-enhanced Raman spectroscopy of nanostructures. *Chem. Soc. Rev.* **2008**, *37* (5), 1025−1041.
(22) Zhang, C.; Zhang, W.; Karadas, F.; et al. Laser-ablation assisted strain engineering of gold nanoparticles for selective electrochemical CO_2 reduction. *Nanoscale* **2022**, *14* (20), 7702−7710.
(23) Rodriguez, P.; Koper, M. T. M. Electrocatalysis on gold. *Phys. Chem. Chem. Phys.* **2014**, *16* (27), 13583−13594.
(24) Shi, C.; Chan, K.; Yoo, J. S.; Nørskov, J. K. Barriers of Electrochemical CO_2 Reduction on Transition Metals. *Org. Process Res. Dev.* **2016**, *20* (8), 1424−1430.
(25) König, M.; Vaes, J.; Klemm, E.; Pant, D. Solvents and Supporting Electrolytes in the Electrocatalytic Reduction of CO_2. *iScience* **2019**, *19*, 135−160.
(26) Mezzavilla, S.; Horch, S.; Stephens, I. E. L.; Seger, B.; Chorkendorff, I. Structure Sensitivity in the Electrocatalytic Reduction of CO_2 with Gold Catalysts. *Angew. Chem., Int. Ed.* **2019**, *58* (12), 3774−3778.
(27) Hasa, B.; Zhao, Y.; Jiao, F. In Situ/Operando Characterization Techniques of Electrochemical CO_2 Reduction. *Annu. Rev. Chem. Biomol. Eng.* **2023**, *14* (1), 165−185.
(28) Kong, C.; Jiang, G.; Sheng, Y.; Liu, Y.; Gao, F.; Liu, F.; Duan, X. Progress on Cu-based metal-organic frameworks for high-efficiency electrochemical CO_2 conversion. *Chem. Eng. J.* **2023**, *460*, No. 141803.
(29) Liu, M.; Pang, Y.; Zhang, B.; et al. Enhanced electrocatalytic CO_2 reduction via field-induced reagent concentration. *Nature* **2016**, *537* (7620), 382−386.
(30) Huang, Y.; Handoko, A. D.; Hirunsit, P.; Yeo, B. S. Electrochemical Reduction of CO_2 Using Copper Single-Crystal Surfaces: Effects of CO* Coverage on the Selective Formation of Ethylene. *ACS Catal.* **2017**, *7* (3), 1749−1756.
(31) Lausche, A. C.; Medford, A. J.; Khan, T. S.; et al. On the effect of coverage-dependent adsorbate−adsorbate interactions for CO methanation on transition metal surfaces. *J. Catal.* **2013**, *307*, 275−282.
(32) Mei, S.; Liang, W. Theoretical Study on the Mechanism of CO* Electrochemical Reduction on Cu(111) under Constant Potential. *Catalysts* **2023**, *13* (6), No. 960.
(33) Sandberg, R. B.; Montoya, J. H.; Chan, K.; Nørskov, J. K. CO-CO coupling on Cu facets: Coverage, strain and field effects. *Surf. Sci.* **2016**, *654*, 56−62.
(34) Katayama, Y.; Nattino, F.; Giordano, L.; et al. An In Situ Surface-Enhanced Infrared Absorption Spectroscopy Study of Electrochemical CO_2 Reduction: Selectivity Dependence on Surface C-Bound and O-Bound Reaction Intermediates. *J. Phys. Chem. C* **2019**, *123* (10), 5951−5963.
(35) Chen, D.-J.; Allison, T. C.; Tong, Y. J. Mechanistic Insights into Electro-Oxidation of Solution CO on the Polycrystalline Gold Surface as Seen by in Situ IR Spectroscopy. *J. Phys. Chem. C* **2016**, *120* (29), 16132−16139.
(36) Tao, Z.; Pearce, A. J.; Mayer, J. M.; Wang, H. Bridge Sites of Au Surfaces Are Active for Electrocatalytic CO_2 Reduction. *J. Am. Chem. Soc.* **2022**, *144* (19), 8641−8648.
(37) Heyes, J.; Dunwell, M.; Xu, B. CO_2 Reduction on Cu at Low Overpotentials with Surface-Enhanced in Situ Spectroscopy. *J. Phys. Chem. C* **2016**, *120* (31), 17334−17341.
(38) Dunwell, M.; Lu, Q.; Heyes, J. M.; et al. The Central Role of Bicarbonate in the Electrochemical Reduction of Carbon Dioxide on Gold. *J. Am. Chem. Soc.* **2017**, *139* (10), 3774−3783.
(39) Dunwell, M.; Luc, W.; Yan, Y.; Jiao, F.; Xu, B. Understanding Surface-Mediated Electrochemical Reactions: CO_2 Reduction and Beyond. *ACS Catal.* **2018**, *8* (9), 8121−8129.
(40) Dunwell, M.; Yang, X.; Yan, Y.; Xu, B. Potential Routes and Mitigation Strategies for Contamination in Interfacial Specific Infrared Spectroelectrochemical Studies. *J. Phys. Chem. C* **2018**, *122* (43), 24658−24664.
(41) Malkani, A. S.; Anibal, J.; Xu, B. Cation Effect on Interfacial CO_2 Concentration in the Electrochemical CO_2 Reduction Reaction. *ACS Catal.* **2020**, *10* (24), 14871−14876.
(42) Chang, X.; Vijay, S.; Zhao, Y.; Oliveira, N. J.; Chan, K.; Xu, B. Understanding the complementarities of surface-enhanced infrared and Raman spectroscopies in CO adsorption and electrochemical reduction. *Nat. Commun.* **2022**, *13* (1), No. 2656.
(43) Jin, L.; Seifitokaldani, A. In Situ Spectroscopic Methods for Electrocatalytic CO_2 Reduction. *Catalysts* **2020**, *10* (5), No. 481.
(44) Zhang, H.; Duan, S.; Radjenovic, P. M.; Tian, Z.-Q.; Li, J.-F. Core−Shell Nanostructure-Enhanced Raman Spectroscopy for Surface Catalysis. *Acc. Chem. Res.* **2020**, *53* (4), 729−739.
(45) Lu, R.; Gan, W.; Wu, B.-h.; Zhang, Z.; Guo, Y.; Wang, H.-f. C−H Stretching Vibrations of Methyl, Methylene and Methine Groups at the Vapor/Alcohol (n = 1−8) Interfaces. *J. Phys. Chem. B* **2005**, *109* (29), 14118−14129.
(46) Wang, H.-F.; Velarde, L.; Gan, W.; Fu, L. Quantitative Sum-Frequency Generation Vibrational Spectroscopy of Molecular Surfaces and Interfaces: Lineshape, Polarization, and Orientation. *Annu. Rev. Phys. Chem.* **2015**, *66* (1), 189−216.
(47) Wang, H.-F.; Gan, W.; Lu, R.; Rao, Y.; Wu, B.-H. Quantitative spectral and orientational analysis in surface sum frequency generation vibrational spectroscopy (SFG-VS). *Int. Rev. Phys. Chem.* **2005**, *24* (2), 191−256.
(48) Ge, A.; Zhou, D.; Inoue, K.-i.; Chen, Y.; Ye, S. Role of Oxygen in Surface Structures of the Solid-Electrolyte Interphase Investigated

by Sum Frequency Generation Vibrational Spectroscopy. *J. Phys. Chem. C* **2020**, *124* (32), 17538−17547.
(49) Braunschweig, B.; Mukherjee, P.; Kutz, R. B.; Wieckowski, A.; Dlott, D. D. Sum-frequency generation of acetate adsorption on Au and Pt surfaces: Molecular structure effects. *J. Chem. Phys.* **2010**, *133* (23), No. 234702.
(50) Huang-fu, Z.-C.; Song, Q. T.; He, Y. H.; et al. Electrochemical CO_2 reduction on Cu and Au electrodes studied using in situ sum frequency generation spectroscopy. *Phys. Chem. Chem. Phys.* **2019**, *21* (45), 25047−25053.
(51) Wallentine, S.; Bandaranayake, S.; Biswas, S.; Baker, L. R. Plasmon-Resonant Vibrational Sum Frequency Generation of Electrochemical Interfaces: Direct Observation of Carbon Dioxide Electroreduction on Gold. *J. Phys. Chem. A* **2020**, *124* (39), 8057−8064.
(52) Wallentine, S.; Bandaranayake, S.; Biswas, S.; Baker, L. R. Direct Observation of Carbon Dioxide Electroreduction on Gold: Site Blocking by the Stern Layer Controls CO_2 Adsorption Kinetics. *J. Phys. Chem. Lett.* **2020**, *11* (19), 8307−8313.
(53) Rebstock, J. A.; Zhu, Q.; Baker, L. R. Comparing interfacial cation hydration at catalytic active sites and spectator sites on gold electrodes: understanding structure sensitive CO_2 reduction kinetics. *Chem. Sci.* **2022**, *13* (25), 7634−7643.
(54) Song, Q.-T.; Huang-Fu, Z. C.; Liu, X.; et al. Electric double layer contribution to sum frequency generation signal from Au electrode. *J. Chem. Phys.* **2023**, *158* (21), No. 214709.
(55) Anfuso, C. L.; Snoeberger, R. C., III; Ricks, A. M.; Liu, W.; Xiao, D.; Batista, V. S.; Lian, T. Covalent Attachment of a Rhenium Bipyridyl CO_2 Reduction Catalyst to Rutile TiO_2. *J. Am. Chem. Soc.* **2011**, *133* (18), 6922−6925.
(56) Rey, N. G.; Dlott, D. D. Structural Transition in an Ionic Liquid Controls CO_2 Electrochemical Reduction. *J. Phys. Chem. C* **2015**, *119* (36), 20892−20899.
(57) Braunschweig, B.; Mukherjee, P.; Haan, J. L.; Dlott, D. D. Vibrational sum-frequency generation study of the CO_2 electrochemical reduction at Pt/EMIM-BF4 solid/liquid interfaces. *J. Electroanal. Chem.* **2017**, *800*, 144−150.
(58) Ratschmeier, B.; Kemna, A.; Braunschweig, B. Role of H_2O for CO_2 Reduction Reactions at Platinum/Electrolyte Interfaces in Imidazolium Room-Temperature Ionic Liquids. *ChemElectroChem* **2020**, *7* (7), 1765−1774.
(59) Zhu, Q.; Wallentine, S. K.; Deng, G.-H.; Rebstock, J. A.; Baker, L. R. The Solvation-Induced Onsager Reaction Field Rather than the Double-Layer Field Controls CO_2 Reduction on Gold. *JACS Au* **2022**, *2* (2), 472−482.
(60) Zhuang, X.; Miranda, P. B.; Kim, D.; Shen, Y. R. Mapping molecular orientation and conformation at interfaces by surface nonlinear optics. *Phys. Rev. B* **1999**, *59* (19), No. 12632.
(61) Li, X.; Pramhaas, V.; Rameshan, C.; Blaha, P.; Rupprechter, G. Coverage-Induced Orientation Change: CO on Ir(111) Monitored by Polarization-Dependent Sum Frequency Generation Spectroscopy and Density Functional Theory. *J. Phys. Chem. C* **2020**, *124* (33), 18102−18111.
(62) van Gisbergen, S. J. A.; Snijders, J. G.; Baerends, E. J. Calculating frequency-dependent hyperpolarizabilities using time-dependent density functional theory. *J. Chem. Phys.* **1998**, *109* (24), 10644−10656.
(63) Gameel, K. M.; Sharafeldin, I. M.; Abourayya, A. U.; Biby, A. H.; Allam, N. K. Unveiling CO adsorption on Cu surfaces: new insights from molecular orbital principles. *Phys. Chem. Chem. Phys.* **2018**, *20* (40), 25892−25900.
(64) Costentin, C.; Drouet, S.; Robert, M.; Savéant, J.-M. Turnover Numbers, Turnover Frequencies, and Overpotential in Molecular Catalysis of Electrochemical Reactions. Cyclic Voltammetry and Preparative-Scale Electrolysis. *J. Am. Chem. Soc.* **2012**, *134* (27), 11235−11242.
(65) Kozuch, S.; Martin, J. M. L. "Turning Over" Definitions in Catalytic Cycles. *ACS Catal.* **2012**, *2* (12), 2787−2794.
(66) Bae, G.; Kim, H.; Choi, H.; et al. Quantification of Active Site Density and Turnover Frequency: From Single-Atom Metal to Nanoparticle Electrocatalysts. *JACS Au* **2021**, *1* (5), 586−597.
(67) Zagal, J. H.; Specchia, S.; Atanassov, P. Mapping transition metal-MN4 macrocyclic complex catalysts performance for the critical reactivity descriptors. *Curr. Opin. Electrochem.* **2021**, *27*, No. 100683.
(68) Araujo, R. B.; Rodrigues, G. L. S.; dos Santos, E. C.; Pettersson, L. G. M. Adsorption energies on transition metal surfaces: towards an accurate and balanced description. *Nat. Commun.* **2022**, *13* (1), No. 6853.
(69) Choi, C.; Kwon, S.; Cheng, T.; et al. Highly active and stable stepped Cu surface for enhanced electrochemical CO_2 reduction to C2H4. *Nat. Catal.* **2020**, *3* (10), 804−812.
(70) Ye, Y.; Yang, H.; Qian, J.; et al. Dramatic differences in carbon dioxide adsorption and initial steps of reduction between silver and copper. *Nat. Commun.* **2019**, *10* (1), No. 1875.
(71) Gajdoš, M.; Hafner, J. CO adsorption on Cu(111) and Cu(001) surfaces: Improving site preference in DFT calculations. *Surf. Sci.* **2005**, *590* (2), 117−126.
(72) Hensley, A. J. R.; Therrien, A. J.; Zhang, R.; Marcinkowski, M. D.; Lucci, F. R.; Sykes, E. C. H.; McEwen, J.-S. CO Adsorption on the "29" CuxO/Cu(111) Surface: An Integrated DFT, STM, and TPD Study. *J. Phys. Chem. C* **2016**, *120* (44), 25387−25394.
(73) Wang, H.; Yan, E. C. Y.; Liu, Y.; Eisenthal, K. B. Energetics and Population of Molecules at Microscopic Liquid and Solid Surfaces. *J. Phys. Chem. B* **1998**, *102* (23), 4446−4450.
(74) Surplice, N. A.; Brearley, W. The adsorption of carbon monoxide, ammonia, and wet air on gold. *Surf. Sci.* **1975**, *52* (1), 62−74.
(75) Gottfried, J. M.; Schmidt, K. J.; Schroeder, S. L. M.; Christmann, K. Adsorption of carbon monoxide on Au(110)-(1 × 2). *Surf. Sci.* **2003**, *536* (1), 206−224.
(76) Kottke, M. L.; Greenler, R. G.; Tompkins, H. G. An infrared spectroscopic study of carbon monoxide adsorbed on polycrystalline gold using the reflection-absorption technique. *Surf. Sci.* **1972**, *32* (1), 231−243.
(77) Ruggiero, C.; Hollins, P. Interaction of CO molecules with the Au(332) surface. *Surf. Sci.* **1997**, *377*−*379*, 583−586.
(78) Kim, J.; Samano, E.; Koel, B. E. CO Adsorption and Reaction on Clean and Oxygen-Covered Au(211) Surfaces. *J. Phys. Chem. B* **2006**, *110* (35), 17512−17517.
(79) Piccolo, L.; Loffreda, D.; Aires, F. J. C. S.; Deranlot, C.; Jugnet, Y.; Sautet, P.; Bertolini, J. C. The adsorption of CO on Au(111) at elevated pressures studied by STM, RAIRS and DFT calculations. *Surf. Sci.* **2004**, *566*−*568*, 995−1000.
(80) Shubina, T. E.; Hartnig, C.; Koper, M. T. M. Density functional theory study of the oxidation of CO by OH on Au(110) and Pt(111) surfaces. *Phys. Chem. Chem. Phys.* **2004**, *6* (16), 4215−4221.
(81) Abild-Pedersen, F.; Andersson, M. P. CO adsorption energies on metals with correction for high coordination adsorption sites − A density functional study. *Surf. Sci.* **2007**, *601* (7), 1747−1753.
(82) Yim, W.-L.; Nowitzki, T.; Necke, M.; et al. Universal Phenomena of CO Adsorption on Gold Surfaces with Low-Coordinated Sites. *J. Phys. Chem. C* **2007**, *111* (1), 445−451.
(83) Koverga, A. A.; Frank, S.; Koper, M. T. M. Density Functional Theory study of electric field effects on CO and OH adsorption and co-adsorption on gold surfaces. *Electrochim. Acta* **2013**, *101*, 244−253.
(84) Zeng, Z.; Greeley, J. Theoretical study of CO adsorption on Au catalysts under environmental catalytic conditions. *Catal. Commun.* **2014**, *52*, 78−83.
(85) Vijay, S.; Hogg, T. V.; Ehlers, J.; et al. Interaction of CO with Gold in an Electrochemical Environment. *J. Phys. Chem. C* **2021**, *125* (32), 17684−17689.
(86) Li, X.; Haunold, T.; Werkovits, S.; Marks, L. D.; Blaha, P.; Rupprechter, G. CO Adsorption and Disproportionation on Smooth and Defect-Rich Ir(111). *J. Phys. Chem. C* **2022**, *126* (15), 6578−6589.

https://doi.org/10.1021/jacs.5c04276
J. Am. Chem. Soc. 2025, 147, 19101−19112

(87) Li, X.; Rupprechter, G. Sum frequency generation spectroscopy in heterogeneous model catalysis: a minireview of CO-related processes. *Catal. Sci. Technol.* **2021**, *11* (1), 12−26.
(88) Li, X.; Roiaz, M.; Pramhaas, V.; Rameshan, C.; Rupprechter, G. Polarization-Dependent SFG Spectroscopy of Near Ambient Pressure CO Adsorption on Pt(111) and Pd(111) Revisited. *Top. Catal.* **2018**, *61* (9), 751−762.
(89) Kong, X.; Zhao, J.; Ke, J.; et al. Understanding the Effect of *CO Coverage on C−C Coupling toward CO_2 Electroreduction. *Nano Lett.* **2022**, *22* (9), 3801−3808.
(90) Hou, J.; Chang, X.; Li, J.; Xu, B.; Lu, Q. Correlating CO Coverage and CO Electroreduction on Cu via High-Pressure in Situ Spectroscopic and Reactivity Investigations. *J. Am. Chem. Soc.* **2022**, *144* (48), 22202−22211.
(91) Zhan, C.; Dattila, F.; Rettenmaier, C.; et al. Revealing the CO Coverage-Driven C−C Coupling Mechanism for Electrochemical CO_2 Reduction on Cu_2O Nanocubes via Operando Raman Spectroscopy. *ACS Catal.* **2021**, *11* (13), 7694−7701.
(92) Rettenmaier, C.; Herzog, A.; Casari, D.; et al. Operando insights into correlating CO coverage and Cu−Au alloying with the selectivity of Au NP-decorated Cu_2O nanocubes during the electrocatalytic CO_2 reduction. *EES Catal.* **2024**, *2* (1), 311−323.
(93) Chang, X.; Xiong, H.; Lu, Q.; Xu, B. Mechanistic Implications of Low CO Coverage on Cu in the Electrochemical CO and CO_2 Reduction Reactions. *JACS Au* **2023**, *3* (11), 2948−2963.
(94) Yao, Y.; Shi, T.; Chen, W.; et al. A surface strategy boosting the ethylene selectivity for CO_2 reduction and in situ mechanistic insights. *Nat. Commun.* **2024**, *15* (1), No. 1257.
(95) Vos, R. E.; Kolmeijer, K. E.; Jacobs, T. S.; van der Stam, W.; Weckhuysen, B. M.; Koper, M. T. M. How Temperature Affects the Selectivity of the Electrochemical CO_2 Reduction on Copper. *ACS Catal.* **2023**, *13* (12), 8080−8091.
(96) Chen, Y.; Li, C. W.; Kanan, M. W. Aqueous CO_2 Reduction at Very Low Overpotential on Oxide-Derived Au Nanoparticles. *J. Am. Chem. Soc.* **2012**, *134* (49), 19969−19972.
(97) Zhu, W.; Michalsky, R.; Metin, Ö.; et al. Monodisperse Au Nanoparticles for Selective Electrocatalytic Reduction of CO_2 to CO. *J. Am. Chem. Soc.* **2013**, *135* (45), 16833−16836.
(98) Zhang, B. A.; Costentin, C.; Nocera, D. G. On the Conversion Efficiency of CO_2 Electroreduction on Gold. *Joule* **2019**, *3* (7), 1565−1568.
(99) Marcandalli, G.; Monteiro, M. C. O.; Goyal, A.; Koper, M. T. M. Electrolyte Effects on CO_2 Electrochemical Reduction to CO. *Acc. Chem. Res.* **2022**, *55* (14), 1900−1911.
(100) Liu, X.; Monteiro, M. C. O.; Koper, M. T. M. Interfacial pH measurements during CO_2 reduction on gold using a rotating ring-disk electrode. *Phys. Chem. Chem. Phys.* **2023**, *25* (4), 2897−2906.
(101) Narayanaru, S.; Chinnaiah, J.; Phani, K. L.; Scholz, F. pH dependent CO adsorption and roughness-induced selectivity of CO_2 electroreduction on gold surfaces. *Electrochim. Acta* **2018**, *264*, 269−274.
(102) Speelman, R.; Marker, E. J.; Geiger, F. M. Quantifying Stern layer water alignment before and during the oxygen evolution reaction. *Sci. Adv.* **2025**, *11* (10), No. eado8536.
(103) Shang, H.; Wallentine, S. K.; Hofmann, D. M.; Zhu, Q.; Murphy, C. J.; Baker, L. R. Effect of surface ligands on gold nanocatalysts for CO_2 reduction. *Chem. Sci.* **2020**, *11* (45), 12298−12306.
(104) Wang, X.; Ou, P.; Wicks, J.; et al. Gold-in-copper at low *CO coverage enables efficient electromethanation of CO_2. *Nat. Commun.* **2021**, *12* (1), No. 3387.
(105) Todorova, T. K.; Schreiber, M. W.; Fontecave, M. Mechanistic Understanding of CO_2 Reduction Reaction (CO_2RR) Toward Multicarbon Products by Heterogeneous Copper-Based Catalysts. *ACS Catal.* **2020**, *10* (3), 1754−1768.
(106) Liu, X.; Xiao, J.; Peng, H.; Hong, X.; Chan, K.; Nørskov, J. K. Understanding trends in electrochemical carbon dioxide reduction rates. *Nat. Commun.* **2017**, *8* (1), No. 15438.
(107) Alsunni, Y. A.; Alherz, A. W.; Musgrave, C. B. Electrocatalytic Reduction of CO_2 to CO over Ag(110) and Cu(211) Modeled by Grand-Canonical Density Functional Theory. *J. Phys. Chem. C* **2021**, *125* (43), 23773−23783.
(108) Zuo, Z.; Huang, W.; Han, P.; Li, Z. Adsorption of CO on Cu (110) and (100) surfaces using COSMO-based DFT. *J. Mol. Model.* **2009**, *15* (9), 1079−1083.
(109) Zhang, D.; Jansen, C.; Berg, O. T.; Bakker, J. M.; Meyer, J.; Kleyn, A. W.; Juurlink, L. B. F. RAIRS Characterization of CO and O Coadsorption on Cu(111). *J. Phys. Chem. C* **2022**, *126* (31), 13114−13121.
(110) Sambare, A. A.; Pawar, R.; Shirsat, M. A DFT investigation on transition metal (Co, Cr, Cu, Mn, Mo and Nb)-doped bismuth ferrite oxide ($BiFeO_3$) for CO gas adsorption. *Theor. Chem. Acc.* **2023**, *142* (7), No. 61.
(111) Hou, X.; Qi, L.; Li, W.; Zhao, J.; Liu, S. Theoretical study on water behavior on the copper surfaces. *J. Mol. Model.* **2021**, *27* (5), No. 149.
(112) Yu, X.; Zhang, X.; Wang, S.; Feng, G. A computational study on water adsorption on $Cu_2O(111)$ surfaces: The effects of coverage and oxygen defect. *Appl. Surf. Sci.* **2015**, *343*, 33−40.

https://doi.org/10.1021/jacs.5c04276
J. Am. Chem. Soc. 2025, 147, 19101−19112